RESEARCH



Plasmonic Interaction of Gold Nanoparticles with the Anti-hypoglycemic Medicament Metformin

Artur L. Hennemann¹ · Miguel D. Ramos Jr¹ · Luca M. Sihn¹ · Marcelo Nakamura¹ · Koiti Araki¹ · Henrique E. Toma¹

Received: 4 December 2023 / Accepted: 29 April 2024 / Published online: 6 May 2024 © The Author(s), under exclusive licence to Springer Science+Business Media, LLC, part of Springer Nature 2024

Abstract

Metformin (MF) is one of the most important medicaments in the market and has been extensively employed in treating type 2 diabetes. In this work, we have observed that, because of its positive charge, MF interacts with negatively charged gold nanoparticles, leading to agglomeration even at low concentrations ($<0.01~\text{mmol}~\text{L}^{-1}$). This is accompanied by the rise of a plasmon coupling band at 645 nm, allowing its colorimetric monitoring with a limit of detection, LOD, of 1.9 μ mol L⁻¹. However, above 0.01 mmol L⁻¹, aggregation takes place, shifting the plasmonic band to 700 nm. Consequently, in this range of concentration, the optical correlation departs from that observed in the agglomeration regime. Therefore, for a critical evaluation, a systematic monitoring of the spectral changes is required to differentiate between the agglomeration and aggregation regimes, as reported in this work. The interaction of metformin with gold nanoparticles has also been monitored by Raman spectroscopy, through the SERS effect. The large enhancement of the Raman signals promoted by the plasmonic nanoparticles improved the detection limit to 0.093 μ mol L⁻¹. While monitoring the plasmonic band has inherently a low specificity, the Raman technique provides an unequivocal detection of metformin, based on its characteristic vibrational profiles.

Keywords Metformin · DLS · Plasmonic nanoparticles · Raman spectroscopy · SERS

Introduction

Metformin (MF) is one of the most important drugs in the market for the treatment of type 2 diabetes mellitus [1–4] being consumed daily by 200 million patients [3]. This anti-hypoglycemic medicament is capable of increasing the peripheral uptake of glucose, improving the biological efficiency of the available exogenous/endogenous insulin. Metformin has also been tested in other medical applications, such as in weight loss treatment [5]. However, because of its increasing consumption, it is being considered a threat as a contaminant in domestic effluents and aquatic systems [6]. Its concentration in several aquatic species can vary from 1 to 80,000 μmol L⁻¹ [6].

The biguanide structure of metformin (Fig. 1) encompasses five coordinating nitrogen atoms and has attracted

the attention of bioinorganic chemists as a metal-chelating agent displaying biological activity [7, 8]. The molecule exhibits a strong basic character, with pKa = 13.25 and 3.07. Its planar configuration leads to tautomeric structures admitting a single protonation between the central imino groups, stabilized by intramolecular hydrogen bonds. For this reason, metformin is normally found in the cationic form. Its analytical detection has been investigated by several techniques [9, 10], including electrochemical, high-performance liquid chromatography, thin-layer chromatography, and liquid chromatography-mass spectrometry methods [2].

In this work, we have explored the cationic behavior of metformin to interact with negatively charged citrategold nanoparticles. We have observed that the electrostatic interaction is strong enough to induce agglomeration and aggregation. This process can be monitored from the characteristic color changes, with the rise of a plasmon coupling band above 600 nm. Such chromatic changes can be employed as a simple and sensitive colorimetric method for metformin.



Instituto de Química, Universidade de São Paulo, São Paulo, SP, Brazil

Fig. 1 Molecular structure of metformin

Materials and Methods

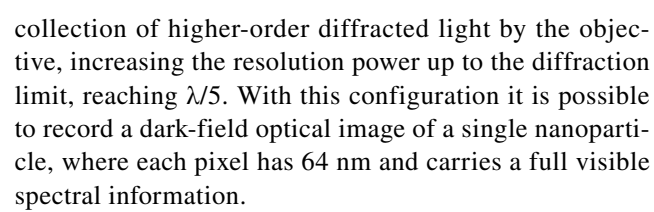
Metformin was obtained from Sigma-Aldrich with high purity and employed as supplied.

The gold nanoparticles (AuNPs) used in the experiments were synthesized by adapting the classical Turkevich method [11, 12]. Initially, 1.7 mL of a 10 mM HAuCl₄ solution was injected into a boiling 2.2 mM sodium citrate solution, with stirring. A pink-to-red solution was formed after 10 min containing the seeds of gold nanoparticles. Then, it was cooled to 90 °C, and an additional portion of 1.7 mL of 10 mM HAuCl₄ was added and stirred for 30 min. This step is intended to promote the nanoparticles growing in a regular form. Finally, a second portion of 1.7 mL of 10 mM HAuCl₄ was added, and the reaction solution was stirred at 90 °C for more than 30 min to accomplish the synthesis. This procedure aims to obtain monodisperse gold nanoparticles, above 30 nm, for improving the detection of the SERS signals using Raman spectroscopy. The solutions were monitored by their extinction spectra, DLS, and zeta size measurements, and used at room temperature, for no longer than a week.

The electronic spectra were recorded on a Hewlett-Packard model 8453-A diode array spectrophotometer, with deuterium and tungsten lamps using rectangular cuvettes with a 1-cm optical path.

Raman measurements were carried out with a Wasatch (WP-785-C-ER-IL-IC f/1.3) high-throughput semi-integrated extended range spectrometer. The equipment is configured for 785-nm Raman measurements (maximum laser output = 450 mW) and 105- μ m fiber optics, with a cooled detector (15 °C), for working on the extended range (2000–3350 cm⁻¹) at a focal distance of 11 mm. The spectrum was acquired using typically 100 mW of power and 1 s integration time, with the sample placed in a 10.0-mm rectangular quartz cuvette.

Darkfield optical and hyperspectral images were obtained with a CytoViva ultra-resolution imaging system, mounted on an Olympus BX51 microscope, providing a suitable detection for recording single-nanoparticle scattering spectra [13]. The sample was prepared by dropcasting the *suspension* on a Nexterion ultraclean glass (Schott). The CytoViva system uses an cardioid annular condenser with a high annular aperture that enables the



A Zetasizer Nano S (Malvern, UK) instrument was employed for measuring dynamic light scattering and zeta potential. The samples were placed in special 10.0-mm cuvettes and illuminated with a He-Ne laser at λ =633 nm, collecting the scattered light at 173°.

For the colorimetric assays involving gold nanoparticles (AuNPs), a stock solution of metformin 1.25 mM was initially prepared. Aliquots of 5 μ L of this solution were added to 5 mL of AuNP suspension, and UV-Vis spectra were recorded after 5 min of agitation. The same procedure was employed for the measurements of the Raman spectra of the aqueous solutions.

Calculation of the limits of detection, LODs, was carried out employing the expression $LOD = 3.3 \times \sigma/S$, where S is the slope of the calibration curve and σ is the standard deviation of the response [14]. Analogously, the limits of quantification, LOQs, were calculated using the expression $LOQ = 10 \times \sigma/S$, or simply LOQ = 3.3 LOD. In all the cases, the spectral data were carefully collected and processed, keeping the same experimental conditions for the experiments, using a blank for baseline subtraction, and measuring directly the absorbance or intensities of the optical signals.

Results and Discussion

Nanoparticle Characterization

The citrate-stabilized gold nanoparticles [15] (AuNPs) exhibited a monomodal distribution in the DLS analyses (Fig. 2) consistent with an average size of 27.13 nm (by number and intensity) and polydispersivity PDII = 0.09.

The typical red colors of the gold nanoparticles are associated with the resonance of the loosely bound electrons, or plasmons, with the exciting radiation, as reported by Mie [16] in 1908. Accordingly, the plasmon excitation at a frequency ω can occur in a radiating or radiationless mode, generating scattering and absorption profiles that are normally embedded in their overall extinction spectra.

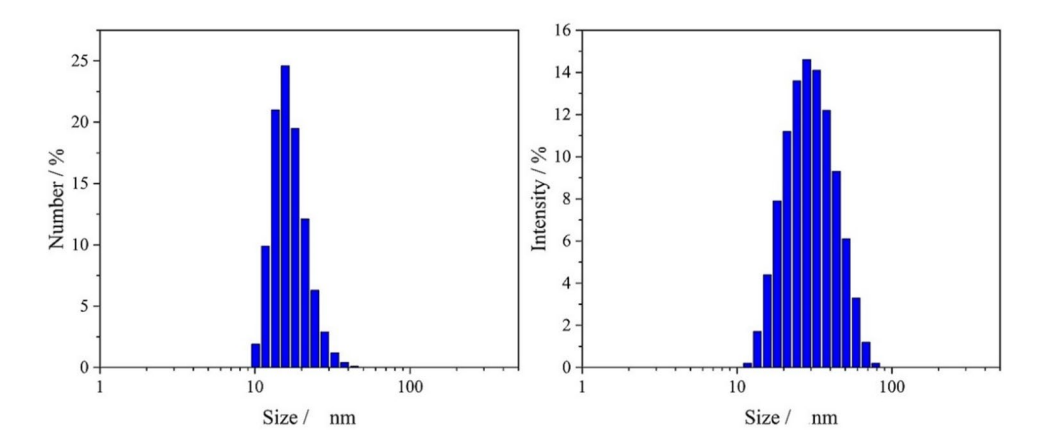
The measured absorbance (A), is given by

$$A = \frac{N\sigma_{ext}d}{2.303}$$

where σ_{ext} is the extinction cross-section encompassing scattering and absorption, d is the sample path length, and N is the nanoparticle concentration. Mie has shown that when



Fig. 2 DLS histograms, monitoring number and intensity, of the citrate-stabilized gold nanoparticles in aqueous solution



the dimensions (r) are much smaller than the light wavelength λ $(2r < \lambda/10)$ only the dipolar oscillations contribute significantly to the extinction cross-section. In this case, the scattering and absorption cross-sections become

$$\sigma_{ext} = 9\left(\frac{\omega}{c}\right) \varepsilon_m^{3/2} V \left(\frac{\varepsilon_2(\omega)}{\left[\varepsilon_1(\omega) + 2\varepsilon_m\right]^2 + \left[\varepsilon_2(\omega)\right]^2}\right)$$

where *V* is the nanoparticle volume, $(4/3)\pi r^3$, ε is the metal dielectric function involving a real (ε_{1} , scattering) and imaginary part (ε_{2} , absorption), given by

$$\epsilon = \epsilon_1(\omega) + i\epsilon_2(\omega)$$

and ε_m is the dielectric of the surrounding medium. The wavelength dependence of the plasmon resonance is associated with the dielectric functions $\varepsilon_1(\omega)$ and $\varepsilon_2(\omega)$, where ω is the frequency of the exciting light.

The extinction cross-sections enclose a resonance condition, leading to a maximum intensity when the denominator approaches zero, i.e., when $\varepsilon = -2\varepsilon_{\rm m}$. The coherent oscillation of the electrons under the influence of electromagnetic radiation generates an oscillating dipole and an enhanced electric near-field (E_s) at the nanoparticle surface, also known as a "hot spot." Hot spots are also generated when the plasmonic nanoparticles become close, as in the case of agglomeration and aggregation. Under such circumstances, the exciting electromagnetic radiation can induce a plasmon coupling between the neighboring nanoparticles, generating an enhanced electric field in the region between two interacting dipoles. This fact is supported by theoretical studies [17–19] showing that in the interparticle region, the electric field is greatly intensified. In addition to the transversal plasmon resonance, the induced longitudinal resonance is responsible for a second peak, leading to a new plasmon coupling band that appears red-shifted in the extinction spectra [20–23].

Metformin exhibits a positive charge under normal conditions and is a good ligand for soft metals [7, 8]. Here,

we have observed that it interacts with gold nanoparticles, leading to the rise of a plasmon coupling band in the visible/near-infrared region (Fig. 3). The interaction is favored electrostatically, due to the negative charges of the citrate-stabilized gold nanoparticles.

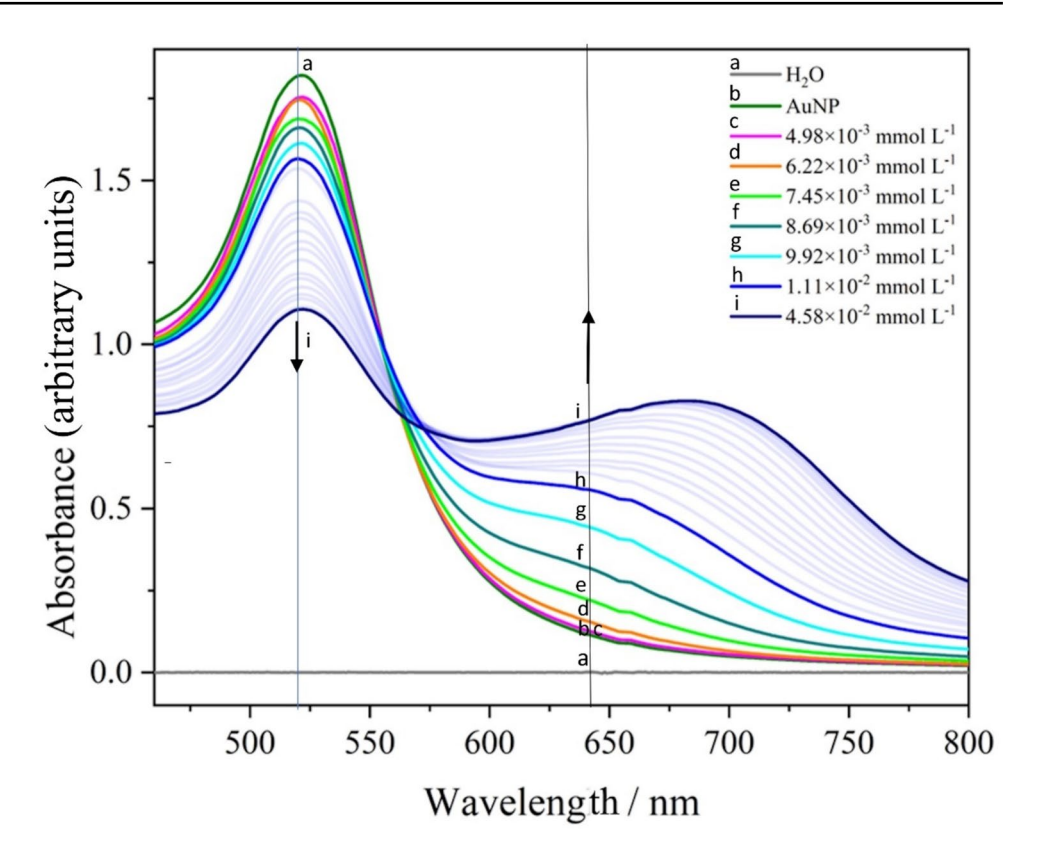
The spectral changes observed during the titration of the gold nanoparticles with metformin have been monitored carefully, as shown in Fig. 3. Initially, there is a decay of the plasmon resonance band at 520 nm, and the rise of a new plasmon coupling band at 645 nm, according to a uniform profile, up to a metformin concentration of 0.011 mol L⁻¹. Above this concentration, the plasmon coupling band starts to move to the red (700 nm) with a small increase in intensity. Therefore, as shown in Fig. 3, there are two distinct spectral reactions, limited by the metformin concentration.

In the first region, corresponding to highly diluted solutions, the gold nanoparticles start agglomerating. Agglomeration refers to a mild, quasi-reversible association of the nanoparticles in solution. Under this condition, the nanoparticles can interact through plasmonic effects, as reflected by the rise of the plasmon coupling band at 645 nm. For analytical purposes, the calibration curve obtained in this region led to a limit of detection (LOD) of 1.99 μ mol L $^{-1}$ and a limit of quantification (LOQ) of 6.58 μ mol L $^{-1}$, as shown in Fig. 4.

The second region starts at a concentration of metformin around 0.1 mmol L⁻¹. Above this limit, the plasmonic band gradually shifts from 645 to 700 nm, indicating the occurrence of aggregation. Aggregation refers to a strong, irreversible association of the nanoparticles. Although the spectral slope is reduced in this region, the noise becomes smaller due to the greatest signal stability accompanying the aggregation kinetics. For this reason, the calibration curve results are quite linear with a small standard error and can be applied for monitoring metformin at more concentrated solutions. However, in this regime, the calculated LOD is meaningless because the extrapolation falls in the first agglomeration region, as shown in Fig. 4. For the sake of completeness, there is also a third region, not shown in Fig. 4, corresponding to



Fig. 3 Spectroscopic changes of the plasmonic spectra of citrate-stabilized gold nanoparticles with the stepwise addition of metformin, showing the decrease of intensity of the plasmon band at 520 and the rise of the plasmon coupling band at 645 nm, followed by the gradual shift to 700 nm, indicating two association regimes, ascribed to agglomeration (a–h) and aggregation (h, i), respectively



the decay of the plasmonic bands due to the precipitation of the aggregated species.

Dynamic Light Scattering and Zeta Potentials

The occurrence of agglomeration and aggregation of the gold nanoparticles has also been monitored by dynamic

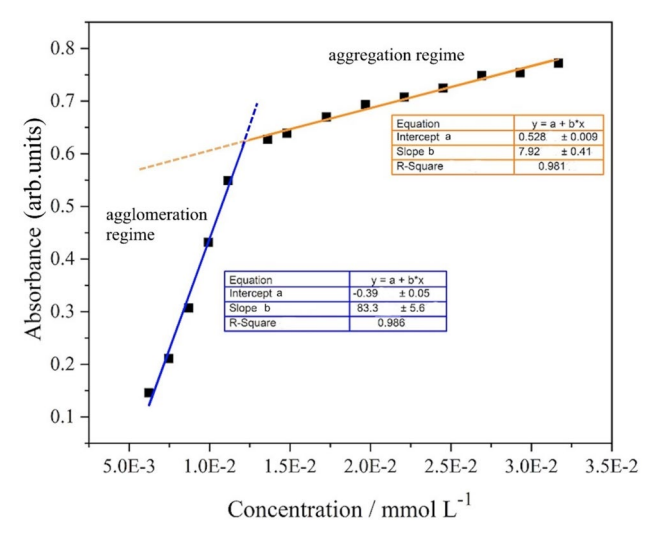


Fig. 4 Calibration plots for the plasmonic detection of metformin at 645 nm, showing the distinct behavior at low (agglomeration) and high (aggregation) concentrations; the experimental errors are embedded in the size of the square dots

light scattering (DLS) and zeta potential measurements (Fig. 5) and can be compared with the spectrophotometric titration shown in Fig. 3. In the range of concentration of MF from 0 to $1\ 10^{-2}$ mmol L⁻¹, corresponding to the first agglomeration region in Fig. 3, the size of the nanoparticles increases slightly from 33 to 40 nm, while the zeta potentials remain nearly constant, around $-30\ mV$

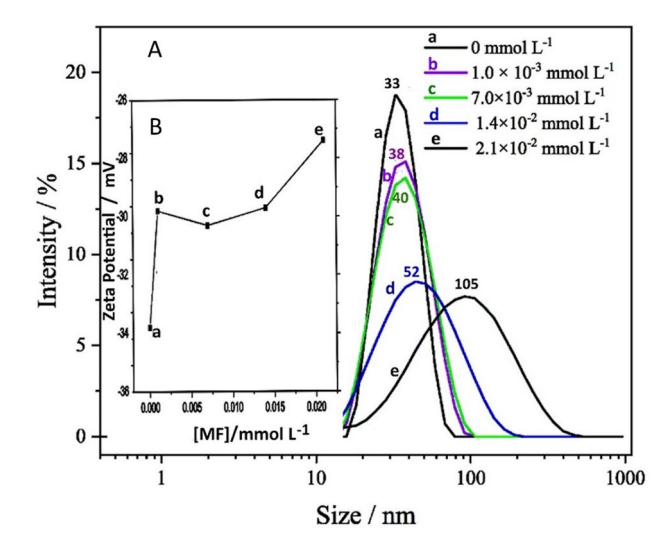


Fig. 5 Dynamic light scattering (**A**) and zeta potential (**B**) measurements for the interaction of citrate-gold nanoparticles and metformin, at several concentrations, in an aqueous solution at room temperature



(Fig. 5a–c. This means that the agglomeration has only a minor influence on the nanoparticle diffusion rates measured by the dynamic light scattering technique. This observation corroborates the idea of agglomeration as a reversible or weak physical association of the particles, despite the pronounced changes observed in the plasmonic bands. Therefore, it is remarkable that the plasmonic interaction can be effective even at the relatively long distances separating the agglomerated nanoparticles.

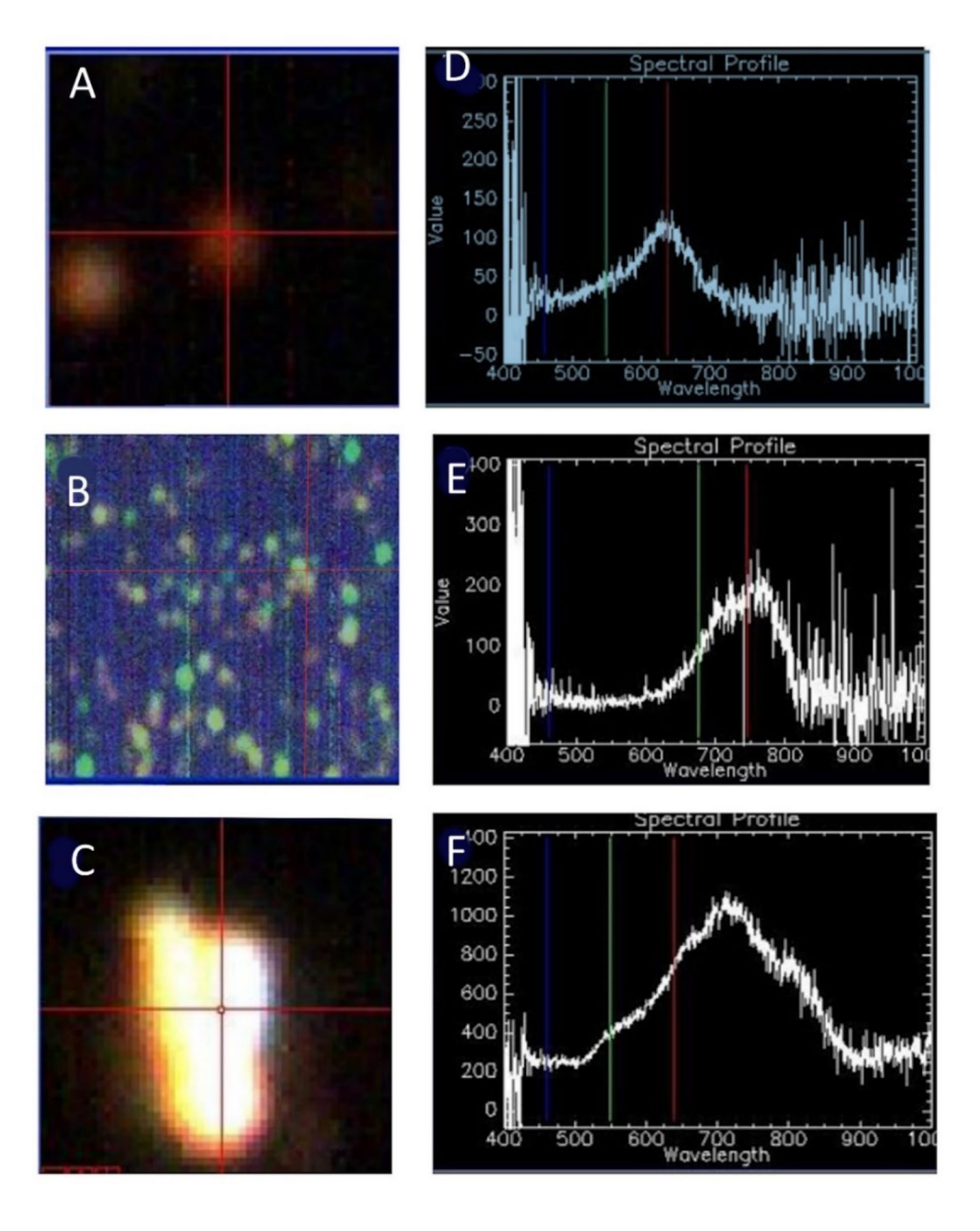
Above 1×10^{-2} mmol L⁻¹, the metformin association with the citrate-gold nanoparticles starts decreasing the electrostatic stability predicted by the DLVO theory, inducing their aggregation. As shown in Fig. 5d, e, in this range of concentration, the measured sizes by DLS increased dramatically from 40 to 105 nm or more, while the zeta potentials became

systematically less negative. The measurements were limited by the precipitation of the aggregated nanoparticles above $4\!\times\!10^{-2}$ mmol $L^{\text{-1}}.$

CytoViva Darkfield Hyperspectral Images

The agglomeration and aggregation of the gold nanoparticles have also been monitored by darkfield microscopy. This technique enables the visualization of single nanoparticles and their scattering spectra. To corroborate the colorimetric analysis, the images of the gold nanoparticles were obtained for very diluted and more concentrated solutions of metformin. The presence of isolated, agglomerated, and aggregated nanoparticles can be seen in Fig. 6, accompanied by their typical scattering spectra.

Fig. 6 Darkfield hyperspectral images for the initial citrate stabilized nanoparticles (**A**) and after the addition of 0.01 (**B**) and 0.03 mmol L⁻¹ **C** of metformin, and **D**–**F** their corresponding light scattering spectra, in the agglomeration (**B**, **E**) and aggregation (**C**, **F**) regimes, respectively





In Fig. 6A and D, the image and scattering spectra correspond to isolated spherical gold nanoparticles, showing a single maximum of around 650 nm. In Fig. 6B, E, the nanoparticles are agglomerated, exhibiting an additional peak associated with the plasmonic coupling. In Fig. 6C, F, the nanoparticles are aggregated, exhibiting multiple quadrupole resonances in the scattering spectra.

SERS Detection of Metformin

Although the interaction with gold nanoparticles provides an interesting way of monitoring metformin with high sensitivity, its analytical detection can be rendered more specific by monitoring the Raman spectra.

Metformin exhibits a characteristic Raman scattering profile, as shown in Fig. 7. The NH₂ vibrational peaks are observed at 601 and 732 cm⁻¹ (ω_{NH2}), followed by the composed C–N+ δ_{NH2} peaks at 942, 1047, and 1089 cm⁻¹ and the composed C=N+ δ_{NH2} peaks at 1283, 1425, 1486, 1598, and 1645 cm⁻¹. The C-H and N-H stretching vibrational peaks are observed at 2945 and 3197 cm⁻¹, respectively.

Although Raman spectroscopy allows monitoring of the molecules in aqueous solution, the signals are usually rather weak because of the small scattering factors involved. For this reason, normal Raman measurements require concentrated solutions, e.g., $> 0.1 \text{ mol L}^{-1}$, which are not suitable for analytical purposes. However, when the molecules are adsorbed onto plasmonic nanoparticles (Ag, Au), the observed Raman spectra can exhibit huge enhancements due to the SERS effect, or surface-enhanced Raman scattering [24–28]. The effect is observed when the exciting radiation

coincides with the plasmon resonance band and is regulated by electromagnetic and chemical mechanisms [15, 29, 30].

The SERS electromagnetic mechanism is viewed as a classical resonance of the nanoparticle electrons with the incident light and leads to Raman enhancement factors from 10⁴ to 10⁸ times for the molecules close to the surface, which are under the influence of the surface plasmon electric field. This effect is particularly strong in the conjunction of two nanoparticles, a region called "hot spot," where the plasmonic coupling enhances the electric field by several orders of magnitude. Therefore, the Raman spectra can become very strong when the plasmonic nanoparticles are in the associated form. On the other hand, the SERS chemical mechanisms require the direct interaction of the molecules with the surface plasmons, giving rise to charge transfer from the ligand HOMO levels to the nanoparticles' Fermi level, or the inverse. This mechanism can be relevant even for isolated nanoparticles, in the absence of hot spots [31, 32].

The Raman spectra of metformin in the presence of gold nanoparticles can be seen in Fig. 8, and the large enhancement observed is consistent with the SERS effect. The spectra exhibit typical NH₂ vibrational peaks at 645 and 744 cm⁻¹ (ω_{NH2}) and composed C=N+ δ_{NH2} major peaks at 1311, 1448, and 93 cm⁻¹, as well as the composed N=C-N vibration at 2120 cm⁻¹. The C-C and C-N stretching vibrations are observed at 945 and 1036 cm⁻¹. The observed spectral pattern at several concentrations is rather similar, being compatible with an electromagnetic mechanism, since there is no evidence of coordination effects on the vibrational peaks, as normally observed in the case of the chemical mechanism [15, 31–35].

Fig. 7 Normal Raman spectrum of MF (0.5 mol L⁻¹) in aqueous solution, recorded at λ_{exc} = 785 nm, showing the typical ranges of the characteristic vibrational peaks

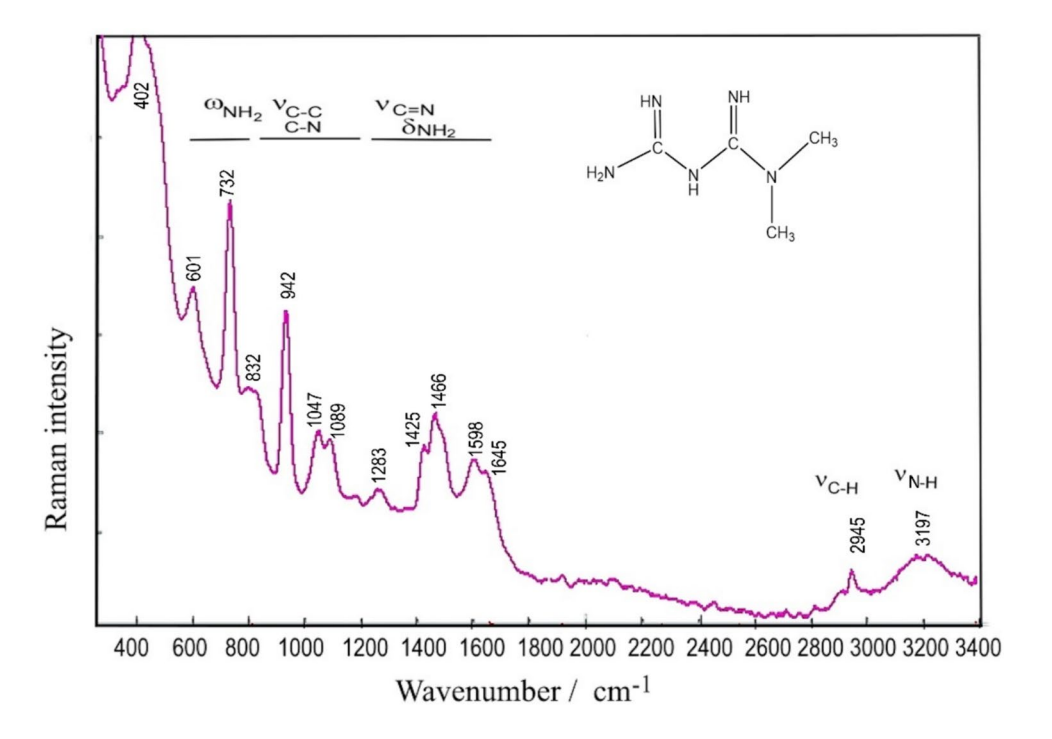
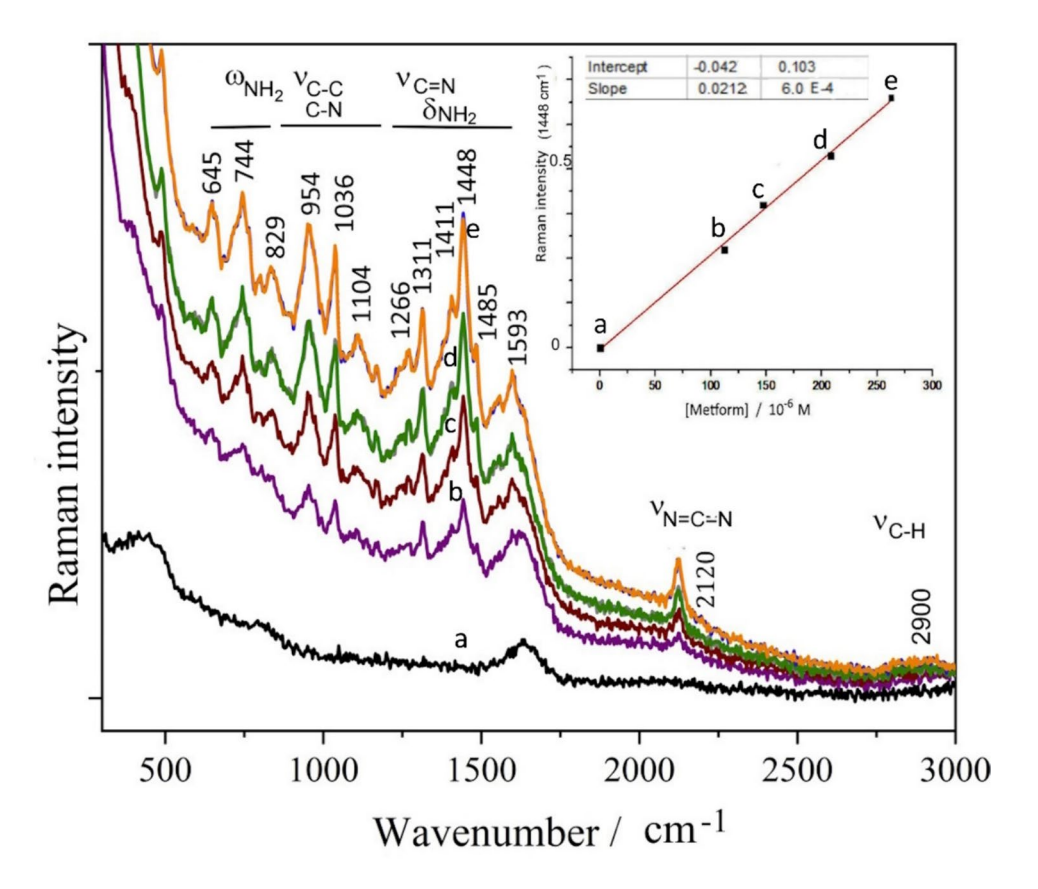




Fig. 8 Raman (SERS) profiles for the titration of citrate AuNPs with metformin in an aqueous solution, at several concentrations of MF, and a typical calibration curve for the peak at 1448 cm⁻¹ (inset), using a laser excitation of 785 nm; the errors are embedded in the size of the square dots



The enhancement factor, EF [36–38], can be estimated from the intensities of the SERS (I_{SERS}) and normal Raman spectra (I_{Raman}) normalized by the relative concentrations of the species under observation (C_{Raman} and C_{SERS}), as expressed by the following equation:

$$EF = \frac{I_{SERS}}{I_{Raman}} \frac{C_{Raman}}{C_{SERS}}$$

By monitoring the vibrational peak observed around $1448 \, \mathrm{cm}^{-1}$, obtained under similar experimental conditions, in the normal Raman and SERS spectra shown in Figs. 7 and 8, respectively, the enhancement factor has been estimated as $1.3 \, (\pm 0.1) \times 10^4$. This result is compatible with the electromagnetic enhancement mechanism.

For analytical purposes, a calibration curve has been elaborated, as shown in Fig. 8 inset, by monitoring the strong peak at 1448 cm $^{-1}$. From the standard deviation $\sigma\!=\!6.0\!\times\!10^{-4}$ and slope = 0.0212, the limit of detection has been calculated as LOD=3.3 x $\sigma/\text{slope}=0.093~\mu\text{mol}$ L $^{-1}$, leading to the limit of quantification LOQ=3.3 and LOD=0.30 μmol L $^{-1}$. In addition to the improved sensibility, the vibrational profiles provide a fingerprint of the molecule, allowing the unequivocal identification of metformin in aqueous solution.

Conclusions

The interaction of metformin with citrate-stabilized gold nanoparticles is favored by its positive charge and leads to pronounced changes in the plasmon resonance spectra. At very small metformin concentrations, the rise of the plasmon coupling band at 645 nm reflects the plasmonic coupling resulting from the nanoparticle's agglomeration. However, at metformin concentrations of 0.01 mmol L⁻¹ and above, a gradual shift of the plasmonic band to 700 nm is observed, corresponding to nanoparticle aggregation.

In the agglomeration regime, a good linearity has been obtained for the optical spectra *versus* the metformin concentration, yielding LOD= $1.9\,\mu\text{mol}\,L^{-1}$. Although the plasmonic method can be considered very sensitive, it should be noted that it lacks specificity, since it only reports the nanoparticle's association phenomena. In this work, by monitoring the plasmonic bands systematically, the agglomeration and aggregation regimes could be discriminated. However, because of their direct influence on the analytical calibration curves, the occurrence of the two regimes cannot be neglected, thus deserving critical consideration.

We have also shown that the interaction of metformin with gold nanoparticles leads to a strong enhancement of the



Raman spectra through the SERS effect. According to the similar SERS spectral profiles obtained as a function of the concentration of metformin, the results are compatible with an electromagnetic mechanism. No additional evidence of metal-substrate coordination, typical of the chemical mechanisms, has been observed. The good linearity of the Raman intensities allowed the construction of a calibration curve, leading to a limit of detection (LOD) of 0.093 $\mu mol \ L^{-1}$ and a limit of quantification of 0.30 $\mu mol \ L^{-1}$. These results are significant, competing with the existing analytical methods in the literature [2, 6, 9, 10]. For instance, the typical LOD values obtained with HPLC methods were in the range of 0.2 to 1.218 $\mu mol \ L^{-1}$ [6]. In addition, the fingerprint identification provided by the Raman spectroscopy is another important aspect of the method.

Author Contribution M.D. Ramos Jr, A. L. Hennemann, and L. M. Sihn performed the analytical and spectrophotometric measurements, M. Nakamura carried out the CytoViva study, K. Araki and H. E. Toma were responsible for conceptualization, Raman investigation, and writing.

Funding The financial support from FAPESP – Fundação de Amparo à Pesquisa do Estado de São Paulo, grant 2018/21489-1, is gratefully acknowledged.

Data Availability No datasets were generated or analyzed during the current study.

Declarations

Competing Interests The authors declare no competing interests.

References

- Ungurianu A, Seremet O, Gagniuc E et al (2019) Preclinical and clinical results regarding the effects of a plant-based antidiabetic formulation versus well-established antidiabetic molecules. Pharmacol Res 150:104522. https://doi.org/10.1016/j.phrs.2019. 104522
- Ambrosio-Albuquerque EP, Cusioli LF, Bergamasco R et al (2021) Metformin environmental exposure: a systematic review. Environ Toxicol Pharmacol 83:103588. https://doi.org/10.1016/j. etap.2021.103588
- Foretz M, Guigas B, Viollet B (2023) Metformin: update on mechanisms of action and repurposing potential. Nat Rev Endocrinol 19:460–476. https://doi.org/10.1038/s41574-023-00833-4
- 4. Bailey CJ (2017) Metformin: historical overview. Diabetologia 60:1566–1576. https://doi.org/10.1007/s00125-017-4318-z
- Shurrab NT, Arafa ESA (2020) Metformin: a review of its therapeutic efficacy and adverse effects. Obes Med 17:100186. https://doi.org/10.1016/j.obmed.2020.100186
- Balakrishnan A, Sillanpää M, Jacob MM, Vo DVN (2022) Metformin as an emerging concern in wastewater: occurrence, analysis and treatment methods. Environ Res. https://doi.org/10.1016/j.envres.2022.113613
- Shahabadi N, Heidari L (2014) Synthesis, characterization and multi-spectroscopic DNA interaction studies of a new platinum

- complex containing the drug metformin. Spectrochim Acta Part Mol Biomol Spectrosc 128:377–385. https://doi.org/10.1016/j.saa. 2014.02.167
- Gopalakrishnan D, Ganeshpandian M, Loganathan R et al (2017) Water soluble Ru(II)-arene complexes of the antidiabetic drug metformin: DNA and protein binding, molecular docking, cytotoxicity, and apoptosis-inducing activity. RSC Adv 7:37706– 37719. https://doi.org/10.1039/c7ra06514k
- Pundir CS, Deswal R, Narwal V, Narang J (2017) Quantitative analysis of metformin with special emphasis on sensors: a review. Curr Anal Chem 14:438–445. https://doi.org/10.2174/1573411013666170907150509
- Tallam AK, Sahithi A, Nuli MV (2023) A review of analytical techniques for determination of metformin: present and perspectives. Int J Heal Care Biol Sci 4:18–24
- Turkevich J, Stevenson PC, Hillier J (1951) A study of the nucleation and growth processes in the synthesis of colloidal gold. Discuss Faraday Soc 11:55–75
- Frens G (1973) Controlled nucleation for regulation of particlesize in monodisperse gold suspensions. Nat Phys Sci 241:20–22
- Vainrub A, Pustovyy O, Vodyanoy V (2006) Resolution of 90 nm (λ/5) in an optical transmission microscope with an annular condenser. Opt Lett 31:2855. https://doi.org/10.1364/OL.31.002855
- Kromidas S (2011) Validation in Analytics. Wiley, VCH, Weinheim, Germany
- Grasseschi D, Toma HE (2017) The SERS effect in coordination chemistry. Coord Chem Rev 333:108–131. https://doi.org/10.1016/j.ccr.2016.11.019
- 16. Mie G (1908) Colloidal solutions. Anallen Der Phys 25:377–445
- Aravind PK, Nitzan A, Metiu H (1981) The interaction between electromagnetic resonances and its role in spectroscopic studies of molecules adsorbed on colloidal particles or metal spheres. Surf Sci 110:189–204. https://doi.org/10.1016/0039-6028(81)90595-1
- Aravind PK, Metiu H (1982) Use of a perfectly conducting sphere to excite the plasmon of a flat surface. 1. Calculation of the local field with applications to surface-enhanced spectroscopy. J Phys Chem 86:5076–5084. https://doi.org/10.1021/j100223a007
- Aravind PK, Metiu H (1983) The effects of the interaction between resonances in the electromagnetic response and sphereplane structure applications to surface-enhanced spectroscopy. Surf Sci 124:506–528. https://doi.org/10.1016/0039-6028(83) 90806-3
- Jain PK, El-Sayed MA (2010) Plasmonic coupling in noble metal nanostructures. Chem Phys Lett 487:153–164. https://doi.org/10. 1016/j.cplett.2010.01.062
- Quinten M, Kreibig U (1986) Optical properties of aggregates of small metal particles. Surf Sci 172:557–577. https://doi.org/10. 1016/0039-6028(86)90501-7
- Halas NJ, Lal S, Chang W-S et al (2011) Plasmons in strongly coupled metallic nanostructures. Chem Rev 111:3913–3961. https://doi.org/10.1021/cr200061k
- Ghosh SK, Pal T (2007) Interparticle coupling effect on the surface plasmon resonance of gold nanoparticles: from theory to applications. Chem Rev 107:4797

 –4862. https://doi.org/10.1021/cr0680282
- 24. Fleischmann M, Hendra PJ, McQuillan AJ (1974) Raman Spectra of pyridine adsorbed at a silver electrode. Chem Phys Lett 26:163–166. https://doi.org/10.1016/0009-2614(74)85388-1
- Albrecht AC (1961) Theory of Raman intensities. J Chem Phys 34:1476
- Albrecht MG, Creighton JA (1977) Anomalously intense Raman spectra of pyridine at a silver electrode. J Am Chem Soc 99:5215–5217
- Jeanmaire DL, Van Duyne RP (1977) Surface Raman spectroelectrochemistry. J Electroanal Chem Interfacial Electrochem 84:1–20. https://doi.org/10.1016/S0022-0728(77)80224-6



- Aroca RF (2006) Surface-enhanced vibrational spectroscopy. John Wiley & Sons, Ltd., Chichester
- Lombardi JR, Birke RL (2012) The theory of surface-enhanced Raman scattering. J Chem Phys 136:144704. https://doi.org/10. 1063/1.3698292
- Lombardi JR, Birke RL (2009) A unified view of surfaceenhanced Raman Scattering. Acc Chem Res 42:734–742
- 31. Zamarion VM, Timm RA, Araki K, Toma HE (2008) Ultrasensitive SERS Nanoprobes for Hazardous Metal ions based on trimercaptotriazine-modified gold nanoparticles. Inorg Chem 47:2934–2936. https://doi.org/10.1021/ic800122v
- Grasseschi D, Parussulo ALA, Zamarion VM et al (2013) How relevant can the SERS effect in isolated nanoparticles be? RSC Adv. https://doi.org/10.1039/c3ra41818a
- Grasseschi D, Parussulo ALA, Zamarion VM et al (2014) SERS studies of isolated and agglomerated gold nanoparticles functionalized with a dicarboxybipyridine-trimercaptotriazine-ruthenium dye. J Raman Spectrosc 45:758–763. https://doi.org/10.1002/jrs.4562
- Grasseschi D, Zamarion VM, Toma HE (2018) Probing the dynamics of dithiooxamide coordinated to gold nanoparticles using SERS. J Raman Spectrosc 49:1478–1486. https://doi.org/ 10.1002/jrs.5398
- 35. Assumpçao AMC, Bonacin JA, Toma SH et al (2014) Probing surface—complex interactions with the bis(4-thienylterpyridine)

- iron(II) complex anchored on TiO2 and gold nanoparticles. Can J Chem 92:918–924. https://doi.org/10.1139/cjc-2014-0025
- Yang Y (2017) SERS enhancement dependence on the diameter of au nanoparticles. J Phys Conf Ser. https://doi.org/10.1088/1742-6596/844/1/012030
- Sacco A, Mangino S, Portesi C et al (2019) Novel approaches in tip-enhanced Raman Spectroscopy: Accurate Measurement of Enhancement factors and Pesticide Detection in Tip Dimer configuration. J Phys Chem C 123:24723–24730. https://doi.org/10. 1021/acs.jpcc.9b07016
- 38. He S, Chua J, Tan EKM, Kah JCY (2017) Optimizing the SERS enhancement of a facile gold nanostar immobilized paper-based SERS substrate. RSC Adv 7:16264–16272. https://doi.org/10.1039/c6ra28450g

Publisher's Note Springer Nature remains neutral with regard to jurisdictional claims in published maps and institutional affiliations.

Springer Nature or its licensor (e.g. a society or other partner) holds exclusive rights to this article under a publishing agreement with the author(s) or other rightsholder(s); author self-archiving of the accepted manuscript version of this article is solely governed by the terms of such publishing agreement and applicable law.

